MULTIFACETED ANALYSIS OF ALUMINUM-COAL ASH-PUMICE COMPOSITES FOR ENHANCED BRAKE DISC SPECIFIC HEAT CAPACITY

Tanimu Kogi Ibrahim[a] *, Danjuma Saleh Yawas[b,c]

[a]Mechanical Engineering Department, Faculty of Engineering, Federal University Wukari, Nigeria
[b]Mechanical Engineering Department, Ahmadu Bello University, Zaria, Nigeria
[c]Shell JV Professorial Chair Office, Mechanical Engineering Department, Ahmadu Bello University, Zaria, Nigeria

Article history
Received
17th May 2024
Revised
22nd December 2024
Accepted
30th January 2025
Published
20th June 2025

*Corresponding email: terrytanimu@yahoo.com

ABSTRACT

The present study investigated the optimization and modelling of some specific process parameters of double stir casting of aluminum, pumice, coal ash (Al-BP-CA) hybrid composites to improve its specific heat capacity for automobile brake disc applications. The constituents were analyzed using X-ray fluorescence (XRF), X-ray diffraction (XRD), thermogravimetric analysis (TGA), and scanning electron microscopy (SEM). The Taguchi approach was utilized to design the experimental runs and optimize the weight composition of reinforcements and stir-casting process parameters. The regression analysis was utilized in developing the mathematical model to forecast the specific heat capacity of the composites. The characterization results revealed that brown pumice and coal ash contained hard and stiff minerals such as SiO_2, Fe_2O_3, and Al_2O_3, making them well-suited as reinforcement in metal matrixes such as aluminum, titanium, and magnesium. According to the thermogravimetric and differential thermal analyses, the aluminum alloy, brown pumice, and coal ash can endure temperatures up to 264.08, 724 °C, and 606.61°C before any deterioration. The optimal specific heat capacities achieved were 824.85 J/kgK (experimental) and 820.48 J/kgK (predicted) by utilizing 7.5 vol% of brown pumice, 5 vol% of coal ash, 400 rpm stirrer speed, 850 °C pouring temperature, and 20 minutes stirring duration. The developed mathematical model shows an excellent level prediction for the specific heat capacity of the composites based on the process parameters and ceramics reinforcement, with R-Square and adjusted R-Square, and predicted R-Square values of 99.27%, 97.25%, and 88.12%, respectively.

Keywords: *Aluminum-Pumice-Coal Ash Hybrid composite; Specific Heat Capacity; Characterization; Taguchi Optimization.*

1.0 INTRODUCTION

In the automotive industry, brake discs stand as vital components ensuring vehicle safety and performance. The importance of specific heat capacity (SHC) in brake discs cannot be overstated, as it directly impacts their ability to manage heat generated during braking. Specific heat capacity governs the disc's thermal stability, determining how efficiently it can absorb and dissipate heat energy. High specific heat capacity enables brake discs to resist temperature fluctuations and mitigate thermal degradation, ensuring reliable braking performance under varying conditions. Additionally, specific heat capacity influences the

DOI 10.11113/jm.v48.509

disc's thermal conductivity, which dictates how quickly heat is transferred away from the braking surface. This balance of properties is crucial for maintaining consistent braking efficacy and preventing issues like brake fade, ultimately enhancing vehicle safety and driver confidence [1,2]. It is essential for manufacturers to carefully consider these factors when designing brake systems.

Several studies have highlighted the need to improve the thermal performance of brake discs, but there is some divergence in approaches. Traditional brake discs made from cast iron have been praised for their durability and performance; however, their high weight has prompted researchers to explore alternative materials. Recent studies have largely agreed on the potential of aluminum composites (AMCs) as a lightweight, high-performance alternative to cast iron. AMCs, reinforced with materials like silicon carbide or carbon fibers, have been shown to offer superior mechanical and thermal properties, enhancing heat dissipation and reducing brake fade [3]. However, some researchers argue that while AMCs provide weight savings and improved thermal efficiency, their performance under extreme braking conditions remains inconsistent compared to cast iron [4,5]. This discrepancy in performance underlines the need for further research into process optimization and material design to ensure the reliability of AMCs in high-temperature applications.

Among the various methods for making AMCs, stir casting stands out. It involves melting the matrix material (aluminum) and adding the reinforcing material to the molten liquid. The blend is then stirred to ensure that the reinforcements are evenly distributed within the matrix. However, the traditional stir casting method has limitations in terms of the uniformity of the reinforcement distribution, which impacts the overall effectiveness of the brake disc [6].

To overcome this limitation, researchers have been exploring the use of double-stir casting to produce AMCs. Double stir casting involves adding a second stirring process after the initial stirring process to ensure that the reinforcements are uniformly distributed throughout the mixture. This method has been found to produce AMCs with better mechanical and thermal properties than those produced using the traditional stir-casting method [7, 8].

The quality and characteristics of the composite material are greatly influenced by the process parameters utilized during casting. Monitoring and controlling these parameters can influence the reaction synthesis that occurs during the processing of the composite melt. Overcoming challenges such as reinforcement distribution, wettability issues between the matrix and reinforced particles, porosity or gas trapping, and reaction viscosity can be accomplished by meticulously selecting and monitoring the process parameters utilized during casting [6,9,10].

The Taguchi optimization technique is a powerful statistical method extensively utilized to optimize process parameters and enhance product quality. This technique uses orthogonal arrays to minimize the experimental runs needed to determine the optimal process parameters. The Taguchi technique is particularly useful when there are several factors involved, and when it is not feasible to test all possible combinations of these factors [11,12].

In line with growing environmental concerns, there's a notable trend towards exploring non-synthetic reinforcements for brake discs. Pumice and coal ash have emerged as promising alternatives, offered unique thermal and mechanical properties while minimizing environmental impact. Pumice, known for its porous structure and lightweight nature, provides excellent thermal insulation properties and high specific heat capacity. Similarly, coal ash, a by-product of coal carbonization, contains mineral components that reinforce brake disc materials and improve thermal stability [13,14]. By harnessing these natural, renewable materials, automotive manufacturers can create brake discs that are not only high-performing and cost-effective but also environmentally friendly and sustainable. This shift towards non-synthetic reinforcements underscores the industry's commitment to

DOI 10.11113/jm.v48.509

greener manufacturing practices and aligns with broader sustainability initiatives aimed at reducing environmental footprint while maintaining product performance and safety standards [15].

This research aims to improve the specific heat capacity of composites made from aluminum, coal ash, and pumice to use them for automobile brake discs. This was achieved through a detailed analytical approach that includes characterizing and producing the natural reinforcements and composites, optimizing the process parameters and natural reinforcements using Taguchi methods, and establishing predictive models through regression analysis. The aim is to enhance the composite specific heat capacity and understand the relationship between variables and SHC. In addition, ANOVA was conducted to assess the significance of factors and interactions on composite-specific heat capacity. The findings from this research are timely and relevant for both the automotive industry and the broader manufacturing sector. By demonstrating the viability of natural, renewable reinforcements like pumice and coal ash, this study aligns with the global push toward sustainable manufacturing practices. This shift is particularly pertinent in the context of the United Nations' Sustainable Development Goals (SDGs), specifically SDG 9 (Industry, Innovation, and Infrastructure) and SDG 12 (Responsible Consumption and Production). The development of high-performance, cost-effective, and environmentally friendly brake discs supports innovation in industrial processes while reducing environmental impact, making this research a valuable contribution to both the scientific community and the automotive industry.

2.0 EXPERIMENTAL PROCEDURE

2.1 Materials

The materials used to produce the hybrid composite are coal, brown pumice, and aluminum alloy (AA6061). The coal was acquired from a coal mine in Effeche-Akpalli, Benue State, Nigeria. The brown pumice was also extracted from an underground mining site in Biu, Borno State, Nigeria.

2.2 Production of Brown Pumice and Coal Ash Particulates

The brown pumice was washed and dried for 48 hours at 100 °C to remove filth and moisture. Respectively. The aggregates were pulverized with a laboratory mortar and pestle before being processed into powders using a ball milling machine. This manufacturing method aligns with studies by Ibrahim *et al.* [13] and Jayakrishnan and Ramesan [16]. The brown pumice particulates were further sieved per BSI 377:1990 standard into three different particle sizes (90 µm, 56 µm, and 25 µm).

The coals were washed and dried for 48 hours at 100 °C to remove moisture and filth before pulverizing them using a jaw crusher. The pulverized coals were put in a crucible made of graphite and subjected to heating to about 1100 °C in an electrical furnace without any air for 8 hours. After being normalized in the oven, it was processed into powders using a ball milling machine. This method is supported by research by Hassan and Gomes [17] and Sharma *et al.* [18]. The generated carbonized coal underwent further sieving per BSI 377:1990 standard to produce carbonized coal ash particles 25, 53, and 90 µm particle size.

2.3 Experimental Design

Taguchi's design methodology was used to plan experimental runs. In this study, five factors: brown pumice particulate (A) (vol%), coal ash particles (CA) (vol%), stirrer speed (SP) (rpm), stirring duration (SD) (min), pouring temperature (°C), and their four different levels were considered to be studied as shown in Table 1. The reinforcement, stirrer speed, pouring temperature, and stirring duration limits and levels were selected, referencing previous studies conducted by Adebisi & Ndaliman [6]; Kumar & Kumar [19]; Patil & Patil

DOI 10.11113/jm.v48.509

[20]. Minitab-21 software was employed to create the L16 orthogonal array for the 16 experimental trials, shown in Table 2.

Table 1: Reinforcements and stir casting process parameters factors and levels

S/N	Processing Factors	Unit	Factors Designation	Level			
				1	2	3	4
1	Brown Pumice	Vol%	A	2.5	5	7.5	10
2	coal ash	Vol%	B	2.5	5	7.5	10
3	Stirrer Speed	rpm	C	200	300	400	500
4	Pouring Temperature	°C	D	700	750	800	850
5	Stirring Duration	min	E	5	10	15	20

Table 2: Orthogonal array for production of hybrid composite

Experimental Run	Factors				
	A (vol%)	B (vol%)	C (rpm)	D (°C)	E (min)
1	2.5	2.5	200	700	5
2	2.5	5	300	750	10
3	2.5	7.5	400	800	15
4	2.5	10	500	850	20
5	5	2.5	300	800	20
6	5	5	200	850	15
7	5	7.5	500	700	10
8	5	10	400	750	5
9	7.5	2.5	400	850	10
10	7.5	5	500	800	5
11	7.5	7.5	200	750	20
12	7.5	10	300	700	15
13	10	2.5	500	750	15
14	10	5	400	700	20
15	10	7.5	300	850	5
16	10	10	200	800	10

2.4 Hybrid Composites Fabrication

The composites were produced using a two-step stir casting procedure described by Ikubanni *et al.* [21] and Adediran *et al*. [3], using a bottom pouring stir casting machine at SwamEquip, Chennai, India.

Prior to the casting process, the brown pumice and coal ash particles underwent a preheating treatment for 2 hrs at 500 °C per the recommendations of previous investigations by Kumar *et al*. [10], Madhukar *et al*. [22] and Adebisi *et al*. [6] to oxidize and calcine the particle surfaces. Subsequently, the aluminum alloys (AA6061) were fed into the electric furnace and heated to 800 °C to guarantee thorough alloy melting. Before incorporating the preheated reinforcements, the surface dross was initially eliminated. Afterwards, 0.01% NaCl (to eliminate gases) and 1% magnesium powders (to enhance wettability) were introduced into the molten aluminum [23]. The liquid alloy undergoes controlled cooling within the furnace until it reaches a temperature of 610 °C, transitioning into a semisolid state. Subsequently, an automated stainless-steel stirrer coated with a protective layer was lowered into the melted aluminum alloy in the furnace to initiate stirring to form a vortex within the melt. The preheated particulate materials were introduced gradually into the molten slurry at a steady flow rate of 5 grams per minute [24]. Subsequently, the mixture

DOI 10.11113/jm.v48.509

was reheated to the prescribed process parameters as specified in the experimental run of the design plan. To ensure proper solidification, the mold was preheated to approximately 450 °C before receiving the molten metal mixture [24].

For each of the experimental trials, this methodology was adhered to, with careful consideration of the process parameters and the reinforcement percentage as recommended in the design plan [6]. A control (without reinforcement) was also produced to compare the effects of the reinforcement. The experimental setup is shown in Figure 1.

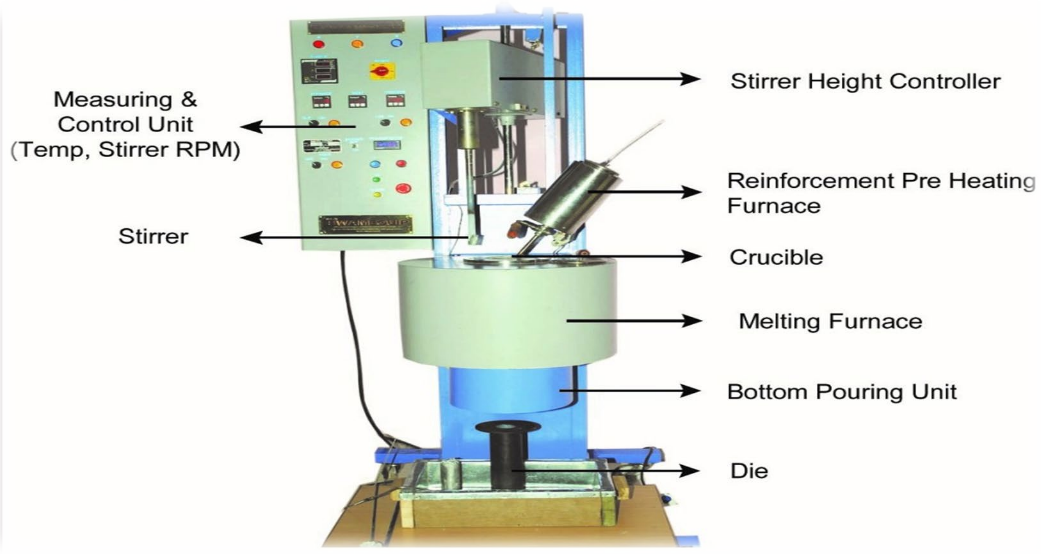

Figure 1: Bottom pouring stir casting machine

2.5 Characterization of the Constituents

Both matrix (aluminum AA6061) and reinforcement (brown pumice and coal ash) were characterized using XRF, SEM-EDS, XRD, and TGA/DTA to determine their chemical composition, morphology, crystalline structure, and thermal stability. These characterizations were done according to the method of Ibrahim *et al*. [31], Ibrahim *et al*. [25] and Ibrahim *et al*. [26].

2.6 Specific Heat Capacity Test

The SHC of the aluminum composite was determined using the mixture method. In this approach, water was poured into a beaker and placed on a hot plate. The sample was then immersed in the water, causing it to boil. The calorimeter and stirrer were initially weighed, and their mass (M_1) was recorded. The calorimeter was filled halfway with cold water, and its mass was rechecked and recorded as M_2. The initial temperature of the cold water was noted as Θ_1, while the final temperature of the boiling water was measured as Θ_2.

Subsequently, the hot sample was swiftly transferred from the beaker into the calorimeter containing the cold water, and it was gently stirred until it reached its maximum temperature, which was recorded as Θ_3. The calorimeter and contents were weighed, and their combined mass was recorded as M_3. Hence, the SHC of the sample was evaluated using Equation 1.

$$\mathrm{S.H.C} = ((\mathrm{M}_c * \mathrm{Cc} + \mathrm{Mw} * \mathrm{Cw})(\Theta_3 - \Theta_2))/(\mathrm{Ms}(\Theta_1 - \Theta_3) \quad (1)$$

Where Mc is the mass of the calorimeter, Mw is the mass of water, Cw is the specific heat capacity of water, Cc is the specific heat capacity of the calorimeter, and Ms is the mass of the sample.

DOI 10.11113/jm.v48.509

2.7 Statistical Analysis and Optimization

The hybrid composites' specific heat capacity was analyzed experimentally using Taguchi optimization and ANOVA with the aid of Minitab-21 software. The study employed a "larger-the-better" objective function in Taguchi optimization to optimize the process parameters that can give us the best composite's specific heat capacity [27,28].

2.8 Confidence Interval (CI)

The confidence interval for this analysis was evaluated using Equation 2.

$$C.I. = \sqrt{f_{\propto(1,d_e)} v_e \left(\frac{1}{m} + \frac{1}{n}\right)} \tag{2}$$

Where $f_{\propto(1,\, d_e)}$ is the F Distribution Critical Values (α=0.05 significance level) between 1 and d_e(which is the degree of freedom of error), gotten from statistical tables, v_e is the variance (mean square) of error, which are obtained from the analysis of variance. N is the number of effective replications. M was evaluated using Equation 3.

$$M = \frac{Total\ number\ of\ experiment}{1 + degree\ of\ freedom\ of\ control\ factors} \tag{3}$$

3.0 RESULTS AND DISCUSSION

3.1 Constituting Materials' XRF Results

The constituents (aluminum alloy (AA6061), brown pumice, and coal ash particles) of the hybrid composites were examined via an XRF analyzer. Tables 3 and 4 present the results of the investigation. The XRF analysis of the aluminum alloy, as shown in Table 3, indicates that aluminum, silicon, and magnesium are the predominant constituents. This finding corroborates the findings of Kareem *et al*. [29] and Ibrahim *et al*. [1].

Table 3: Aluminium's chemical composition

Element	Al	Si	Fe	Cu	Mn	Mg	Zn	Cr	Ti	Ca	others
vol%	97.74	0.61	0.44	0.16	0.02	0.82	0.01	0.07	0.01	0.05	0.06

Table 4 shows the XRF results of the coal ash and pumice particulates. The analysis verified that coal particle ash predominantly consisted of Si, Al, Fe, Ti, and Ca. The major constituents of brown pumice particulates were Si, Fe, Al, Ca, K, and Ti. These outcomes are consistent with the studies undertaken by Ibrahim *et al*. [13] and Dagwa & Adama [30]. The presence of these elements indicates that brown pumice and coal ash particles have the potential to serve as effective particulate reinforcements in metal matrices given their chemical composition, which shares similarities with certain agricultural and industrial residues (bagasse, coconut fiber ash, and banana fibers ash, fly ash, bottom ash, and red mud) [26,32,33].

DOI 10.11113/jm.v48.509

Table 4: Pumice particulate and CA chemical composition

S/n	Elements	Brown pumice (%)	Coal ash Particles (%)
1	O	42.267	46.52
2	Al	7.907	7.556
3	Si	20.594	22.141
4	P	0.288	0.000
5	S	0.074	4.415
6	Cl	0.718	1.721
7	K	4.212	1.130
8	Ca	8.574	2.667
9	Ti	2.140	3.500
10	V	0.084	0.140
11	Cr	0.008	0.170
12	Mn	0.198	0.268
13	Fe	12.348	8.910
14	Co	0.070	0.062
15	Ni	0.010	0.066
16	Cu	0.046	0.147
17	Zn	0.029	0.014
18	Zr	0.157	0.322
19	Nb	0.050	0.054
20	Mo	0.002	0.011
21	Ag	0.027	0.031
22	Ba	0.186	0.123
23	Ta	0.012	0.035

3.2 Constituting Materials' X-ray Powder Diffraction

Based on the XRD patterns of brown pumice particulates (A) displayed in Figure 2, it is evident that the patterns include peaks corresponding to an amorphous quartz (SiO_2) material, along with specific crystalline phases of anorthite ($Ca\ Al_2(SiO_4)_2$) and albite ($NaAlSi_3O_8$). These findings correlate with Ersoy *et al*. [34] and Pinarci and Kocak [35] findings. Upon matching the coal ash particulates (B), distinct phases of SiO_2, graphite, and muscovite ($KAl_2(AlSi_3O_{10})(F,OH)_2$) were identified, as shown in Figure 1. These results are in agreement with other studies by Ibrahim *et al.* [1].

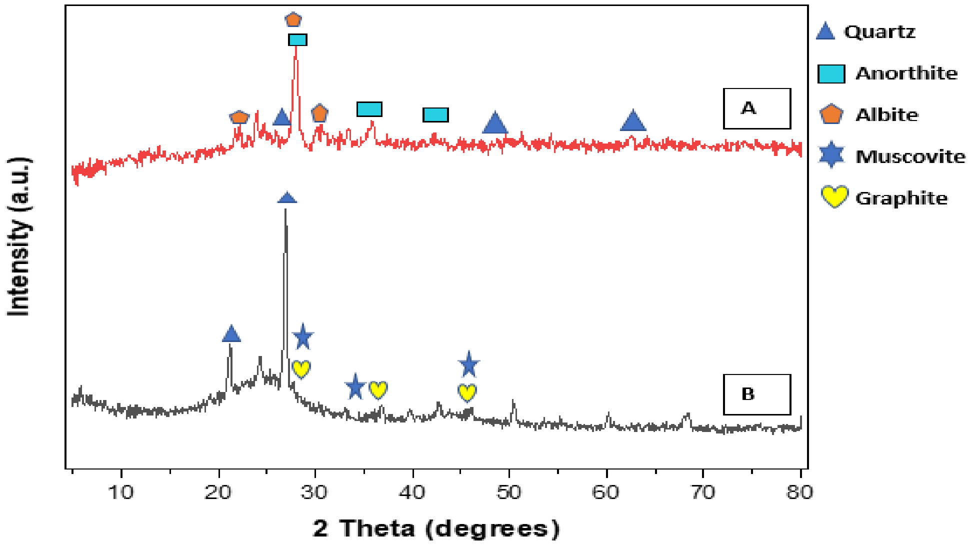

Figure 2: XRD results of pumice and coal ash particulates

3.3 Thermogravimetric and Derivatives of Thermal Analysis of Aluminum Alloy, Brown Pumice, and Coal Ash

Figures 3, 4 and 5 show the results of the thermogravimetric and derivatives of thermal analysis of aluminum alloy, pumice, and coal ash, respectively.

The TGA-DTA curves in Figure 3 demonstrate a two-step weight loss for aluminum alloy when exposed to a nitrogen gas atmosphere and heated within the temperature range of 30°C to 1000°C. The TGA curve in the figure shows a significant drop until it becomes parallel to the temperature axis at approximately 513 °C.

The initial 1.16% weight loss occurs between a temperature of 83.29 and 264.08 °C, which can be linked to the evaporation of the absorbed surface moisture and some volatile matter. The major decompositions of the materials occur in one stage between the temperatures of 264.08 and 513 °C with a mass loss of 81.2%.

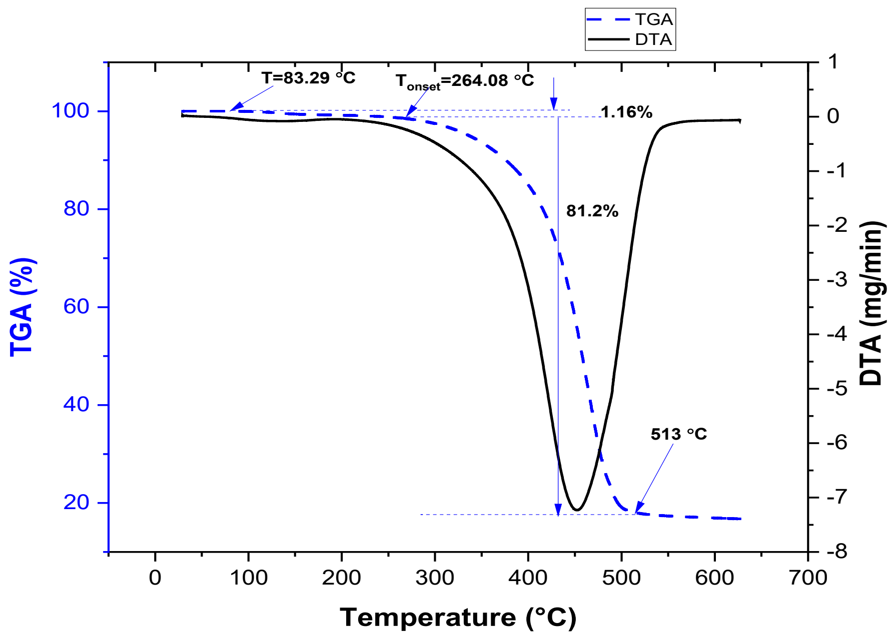

Figure 3: TGA-DTA curves of the aluminum alloy (AA6061)

The TGA-DTA curves in Figure 4 depict a two-step weight loss pattern for brown pumice particulates when exposed to a nitrogen gas atmosphere and heated within the temperature range of 30°C to 1000°C. The TGA curve in the figure demonstrates a substantial decline until it aligns parallel to the temperature axis around 957 °C.

The initial 0.46% weight loss occurs between a temperature of 495.54 and 724 °C was observed, which can be linked to the evaporation of the absorbed surface moisture and some volatile matters. The major decompositions of the materials occur in one stage between 724 and 957 °C with a mass loss of 11.26%. The major decompositions in pumice can be attributed to the thermal decomposition of volatile matters such as sulfur dioxide (SO_2), carbon dioxide (CO_2), nitrogen, and various trace gases that may be present in the volcanic environment during the rock's formation. The lower mass loss in brown pumice particulates is owing to its high melting points (1343 °C) and the presence of TiO_2 (1843 °C) and SiO_2 (1710 °C), the major constituents, compared to the lower melting temperature of the aluminum alloy. This observation is similar to the work of Ibrahim *et al.* [36] and Gencel [37].

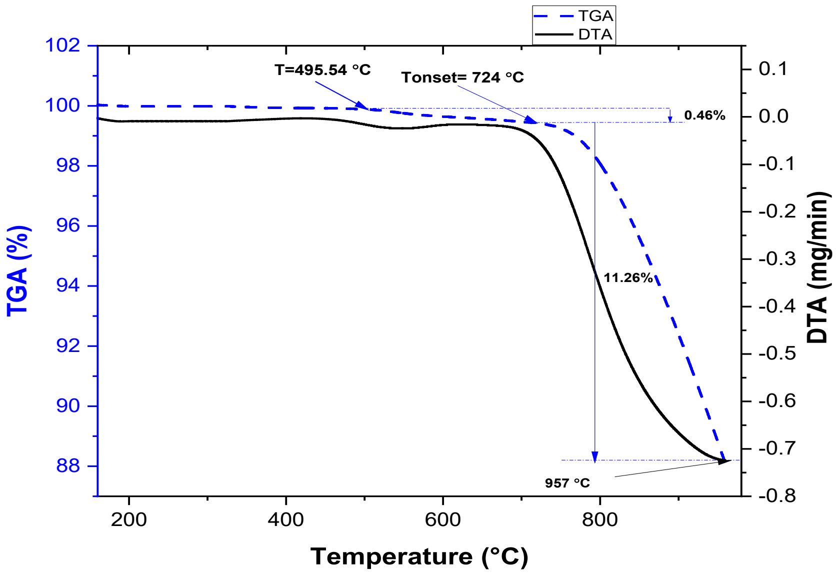

Figure 4: TGA-DTA Curves of the brown pumice particulates

The TGA-DTG curves in Figure 5 demonstrate a three-step weight loss for coal ash particulates when exposed to a nitrogen gas atmosphere and heated within the temperature range of 30°C to 1000°C. The TGA curve in the figure shows a significant drop until it becomes parallel to the temperature axis at approximately 980.04 °C.

The initial 1.2% weight loss occurs between a temperature of 238.67 and 605.51 °C observed, which can be linked to the evaporation of the absorbed surface moisture and volatile matter. The major decompositions of coal ash particulates occur in two stages: The initial phase occurred within the temperature range of 605.51 °C to 840.52 °C, resulting in a mass reduction of 13.68%. Subsequently, the second phase occurred between 840 °C and 980.4 °C, with a mass loss of 24.38%. The first stage of major decomposition in coal ash particulates can be attributed to the volatile components such as water, hydrocarbons, or other gases trapped within the coal particles. The second stage might be due to the decomposition of carbonated minerals into oxides, which release carbon dioxide (CO_2) gas. The reduced mass loss in coal ash particulates is attributed to the elevated melting points of their primary constituents, TiO_2 and SiO_2 (1843 °C and 1710 °C, respectively), in comparison to the lower melting temperature of the aluminum alloy.

DOI 10.11113/jm.v48.509

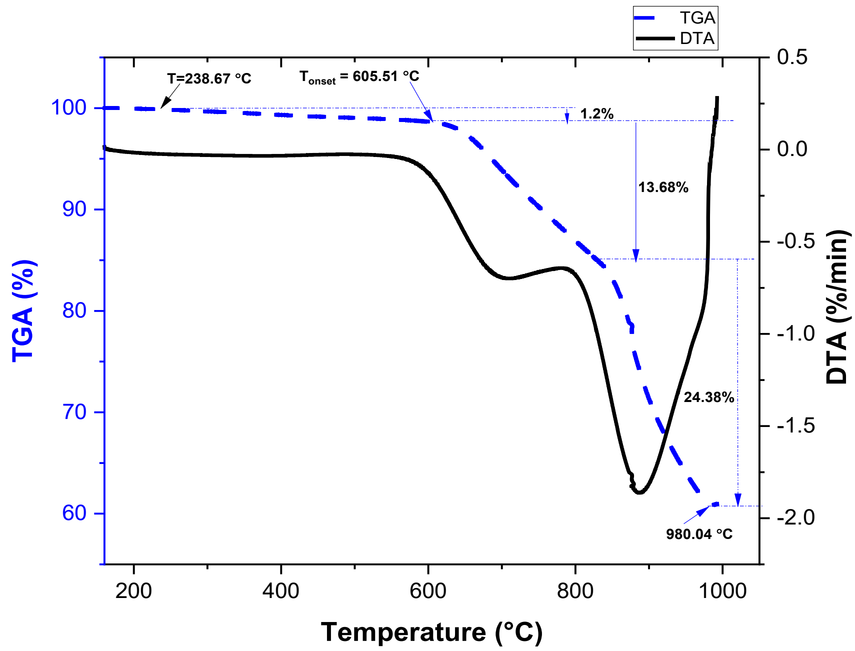

Figure 5: TGA-DTA curves of the coal ash particulates

3.4 Specific Heat Capacity (SHC) Results Analysis of the Hybrid Composite Developed

Table 5 shows the results of a specific heat capacity test performed on sixteen hybrid composites and a control sample, along with their signal-to-noise ratios. From the Table, the highest SHC of 810 J/kgK was recorded at experiment No. 14. The minimum of 599.74 J/kgK was recorded at experiment No. 1. The specific heat capacity (SHC) of the as-cast aluminium alloy (i.e., control) is less than that of the 16-produced hybrid composite, as shown in the Table; this could be attributed to the presence of reinforcements (pumice and carbonated coal) that have a higher specific heat capacity (SHC) compared to the aluminium alloy. This result agrees with some related studies by Shetty *et al*. [38], Hoff *et al*. [39], and Santhosh Kumar *et al*. [40]. They show that the SHC of a composite depends on the constituent SHC, volume fraction, particle size, and distribution of the constituent.

Table 5: Specific heat capacity test results and their respective signal to noise ratio

Runs	Factors					Specific Heat Capacity	
(S/N)	A (wt%)	B (wt%)	C (rpm)	D (°C)	E (min)	Mean (J/kgK)	S/N ratio (dB)
1	2.5	2.5	200	700	5	599.74	55.56
2	2.5	5	300	750	10	600.77	55.57
3	2.5	7.5	400	800	15	634.60	56.05
4	2.5	10	500	850	20	665.52	56.46
5	5	2.5	300	800	20	686.57	56.73
6	5	5	200	850	15	754.56	57.55
7	5	7.5	500	700	10	671.16	56.54
8	5	10	400	750	5	691.87	56.80
9	7.5	2.5	400	850	10	735.75	57.33
10	7.5	5	500	800	5	737.01	57.35

DOI 10.11113/jm.v48.509

Runs	**Factors**					**Specific Heat Capacity**	
(S/N)	**A (wt%)**	**B (wt%)**	**C (rpm)**	**D (°C)**	**E (min)**	**Mean (J/kgK)**	**S/N ratio (dB)**
11	7.5	7.5	200	750	20	761.24	57.63
12	7.5	10	300	700	15	771.03	57.74
13	10	2.5	500	750	15	754.44	57.55
14	10	5	400	700	20	810.28	58.17
15	10	7.5	300	850	5	737.01	57.35
16	10	10	200	800	10	626.62	55.94
Mean						**702.38**	**56.90**
Control (As cast)						**596.08**	

3.5 Taguchi Optimization of Reinforcements and Casting Process Parameters

The higher-the-better objective function was used to observe the optimum and the most influential process parameters in the casting of aluminum hybrid composite. This analysis gave signal-to-noise ratios, main effect plots for the mean of the responses, and that of signal-to-noise ratios, as presented in the discussions below;

3.5.1 Impact of Process Parameters of Stir Casting on the Specific Heat Capacity

Figures 5 to 9 illustrate the influence of pumice particulates, coal ash particles, stirrer speed, pouring temperature, and stirring duration on the specific heat capacity, each in a separate figure, which is discussed in the following subsections.

3.5.1.1 Effect of Pumice Particulates on Specific Heat Capacity

The SHC of the reinforced AMCs is influenced by the addition of pumice particulates, as illustrated in Figure 6. The figure indicates that the specific heat capacity initially increases with an increase in pumice particulate content until it reaches 7.5%, after which it starts decreasing with further addition. The increase in specific heat capacity could be accredited to the even dispersion of the pumice particulates in the aluminum matrix. It can also be attributed to pumice's high specific heat capacity compared to aluminum Al6061. In contrast, the decrease could be attributed to the saturation of the pumice in the matrix since there is less matrix ratio than the reinforcement. This result agrees with some related studies by Hasan *et al*. [41], Cem Okumus *et al*. [42] and Krishna *et al*. [43]. In their studies, they inferred that the SHC of the composite is influenced by the SHC of the constituents; it increases (i.e., if the SHC of the reinforcement is greater than that of the matrix) to the maximum, then with further addition of the reinforcement, it declines. From the analysis, the best (optimum) specific heat capacity for the composite was 751.3 J/kgk at 7.5 wt% pumice particulate content.

DOI 10.11113/jm.v48.509

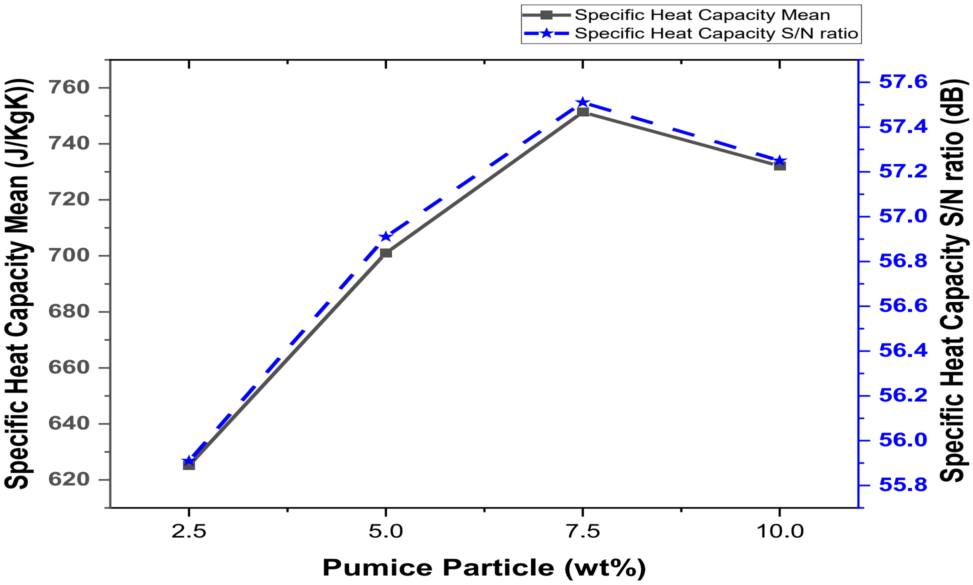

Figure 6: Variation of pumice particulate content on the specific heat capacity of the aluminum hybrid composite

3.5.1.2 Effect of Coal Ash Particulates on Specific Heat Capacity

Figure 7 illustrates the impact of coal ash particulates on the specific heat capacity of the produced AMC. The figure indicates that as the coal ash particle content increases, the specific heat capacity initially increases and reaches a peak value of 725.70 J/kgk. However, with a further increase, the specific heat capacity decreased. The increase in the SHC could be accredited to the uniform distribution of the coal ash within the matrix. However, the reduction observed in the specific heat capacity beyond the peak value could be ascribed to the reinforcement saturation in the matrix. Furthermore, the presence of graphite in coal ash can also be a contributing factor, as reported by Krishna *et al*. [43]. From the analysis, the optimum specific heat capacity of 725.7 J/kgk was observed at 5 wt% coal ash particle content.

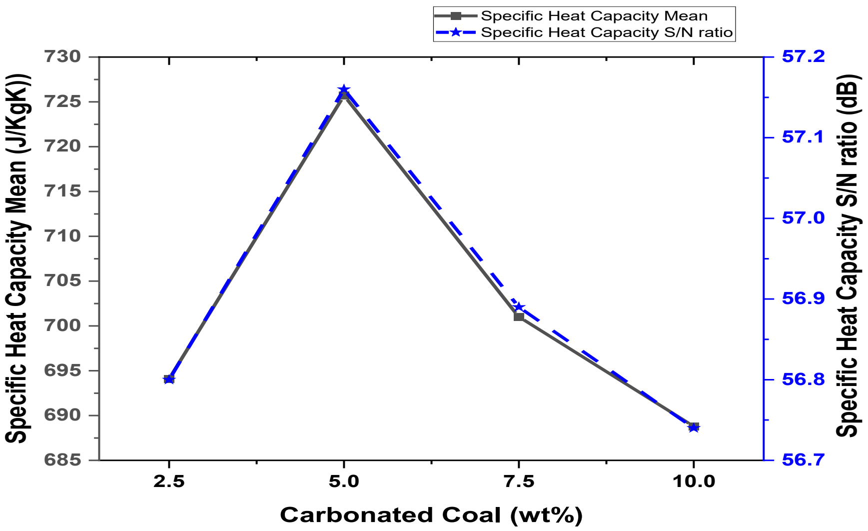

Figure 7: Variation of coal ash particle content on the specific heat capacity of the aluminum hybrid composite

DOI 10.11113/jm.v48.509

3.5.1.3 Effect of Stirrer Speed on Specific Heat Capacity

Figure 8 illustrates that the SHC increases with increasing stirrer speed during casting up to 400 rpm. Beyond this speed, a decrease was observed. The increase may be accredited to the homogeneous dispersion of the reinforcement in the aluminum matrix. In contrast, the observed decrease in SHC could be attributed to the inhomogeneous dispersion of reinforcement particles within the aluminum matrix. This inhomogeneity might be caused by the increased agitation during the stir casting process. At higher agitation levels, the pumice and coal ash particles may cluster together instead of dispersing uniformly. Additionally, the intense stirring could also lead to the entrapment of gas bubbles within the composite material. Both clustering and gas bubbles can act as internal voids, effectively reducing the effective material available to absorb heat, and thereby lowering the overall SHC. This result is similar to the investigations conducted by Khosravi *et al*. [44] and Malau *et al*. [45]. They reported that at higher stirrer speeds, clustering and gas entrapment occur. From the analysis, an optimum of 718.1 J/kgk was observed to be the optimum specific heat capacity at a stirrer speed of 400 rpm.

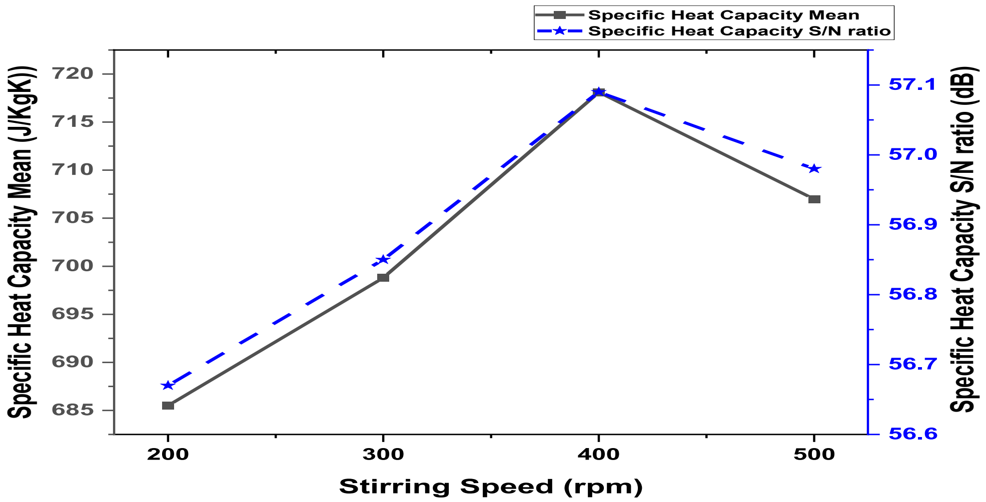

Figure 8: Variation of stirrer speed on the specific heat capacity of the aluminum hybrid composite

3.5.1.4 Effect of Pouring Temperature on Specific Heat Capacity

Figure 9 displays the influence of pouring temperature on the SHC of the aluminum composite. The figure indicates that the specific heat capacity decreased as the pouring temperature increased up to 800 °C. However, with a further increase in pouring temperature, the specific heat capacity also increased. The decrease may be due to the high viscosity of the aluminum melt at a lower temperature, which reduces the wettability of the reinforcements. At the same time, the increase in SHC could be ascribed to the decreased viscosity of the melted aluminum at higher temperatures. The increase in the aluminum melt's viscosity improves the reinforcement's distribution in the matrix and the reinforcement's wettability due to the decrease in the contact angle. This study is consistent with Hashim *et al*. [46] and Ibrahim *et al*. [47]. Their studies suggest that a higher melt temperature reduces the contact angle between the matrix material and the reinforcement particle surfaces. The figure shows an optimum specific heat capacity of 723.20 J/kgK at a pouring temperature of 850 °C.

DOI 10.11113/jm.v48.509

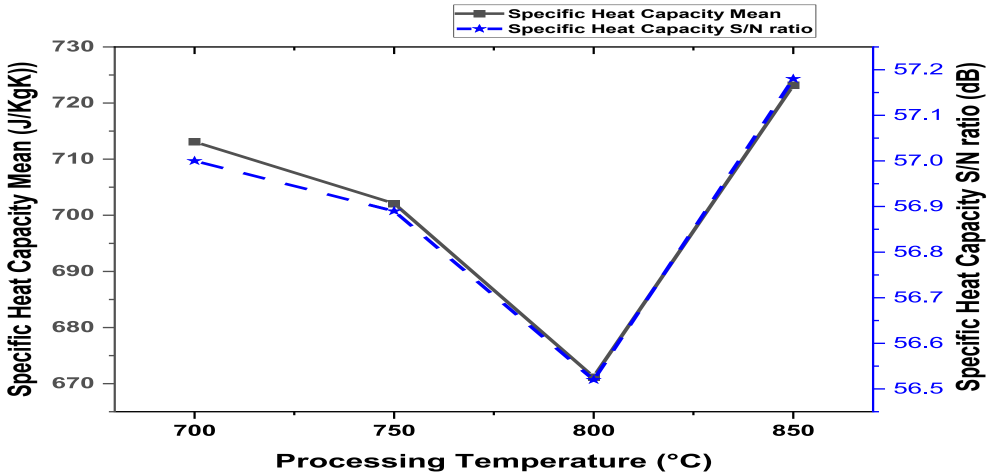

Figure 9: Variation of pouring temperature on the specific heat capacity of the aluminium hybrid composite

3.5.1.5 Effect of Stirring Duration on Specific Heat Capacity

As was observed in Figure 10, the SHC decreases with an increase in the stirring duration of up to 10 min. With further increase in stirring duration, the specific heat capacity started increasing to the maximum value of 730.90 J/kgK. The decrease in specific heat capacity might be attributed to the non-uniform dispersion of the reinforcement in the matrix due to inadequate duration for stirring. In contrast, the increase might be connected to the homogeneous reinforcement's dispersion in the composite due to adequate stirring duration. An optimum SHC of 730.90 J/kgK was observed at a stirring duration of 20 minutes. This finding is similar to Khosravi *et al*. [44] and Karthikeyan *et al*. [48].

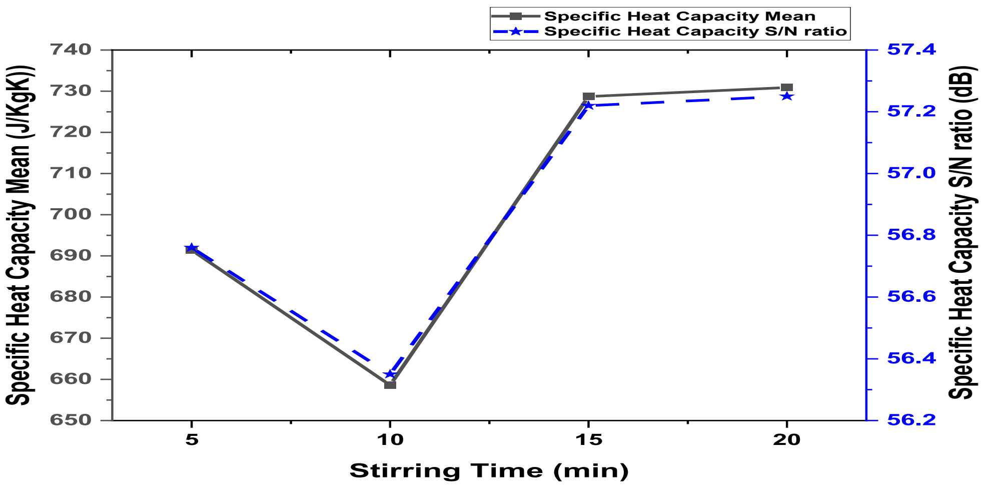

Figure 10: Variation of stirring duration on the specific heat capacity of the aluminum hybrid composite

3.5.2 Optimal Combination and Confirmation Test for the Specific Heat Capacity

From Figure 6 to Figure 10, the optimum reinforcements and process parameters of stir casting for the optimum specific heat capacity are pumice particulates (A) content at 7.5 % (level 3), coal ash particulates (B) at 5 % (level 2), with a Stirrer speed (C) of 400 rpm (level 3), a pouring temperature (D) of 850 °C (level 4), and stirring duration (E) of 20 minutes (level 4). Therefore, the predicted combination of levels for optimum specific heat capacity is denoted as A_3 -B_2-C_3-D_4-E_4.

Based on the best combination of optimal levels of factors, the predicted optimum SHC for the aluminum hybrid composites was 820.48 J/kgK.

DOI 10.11113/jm.v48.509

Table 6 compares predicted and experimental SHC for the optimal processing conditions (A_3-B_2-C_3-D_4-E_4) of the hybrid aluminum matrix composite, including percentage error. From the analysis, a 0.53% experimental error was observed.

Table 6: Confirmatory results comparison at the optimal level

	Optimal process parameter settings	Predicting value	Experimental value	% Error
S/N ratio (dB)	A_3 -B_2-C_3-D_4-E_4	58.28	58.33	0.09
SHC (J/kgK)		820.48	824.85	0.53

3.6 Regression Analysis (Modelling)

The regression model analysis developed the ANOVA table and the mathematical model to predict specific heat capacity. Table 7 which was developed at a confidence level of 95%, shows that the regression model, all the factors, and the interactions were found to be significant to the SHC of the produced hybrid AMC with p-values below 0.05. Among the factors, the coal ash particulates made the highest contribution (21.1%), while the pouring temperature made the least (4.8%).

Table 7: ANOVA for the specific heat capacity of the AMC

Source	DF	Adj SS	Adj MS	F-Value	P-Value	% Contribution
Regression	11	62194.3	5654	49.16	0.001	
A	1	5282.5	5282.5	45.93	0.002	9.1
B	1	12808.8	12808.8	111.38	0.000	22.1
C	1	3780.8	3780.8	32.88	0.005	6.5
D	1	2791.5	2791.5	24.27	0.008	4.8
E	1	2913.8	2913.8	25.34	0.007	5
B*B	1	1915.9	1915.9	16.66	0.015	3.3
C*C	1	447.6	447.6	3.89	0.120	0.8
D*D	1	3967.3	3967.3	34.5	0.004	6.8
E*E	1	5537.8	5537.8	48.15	0.002	9.5
A*C	1	8768.8	8768.8	76.25	0.001	15.1
B*D	1	9339.6	9339.6	81.21	0.001	16.1
Error	4	460	115			0.8
Total	**15**	**58014.4**				**100**

At a 95 per cent confidence level, Table 4.15 shows that only C*C was insignificant, with a p-value greater than 0.05.

From the regression analysis, a model for predicting the specific heat capacity as a function of the stir-casting process parameters was derived, as shown by Equation 4.

$$SHC = 3495 - 46.92\,\mathrm{A} + 184.5\mathrm{B} - 1.398\mathrm{C} - 8.22\mathrm{D} - 15.29 - 1.751\mathrm{B}^2 + 0.000591\mathrm{C}^2 + 0.00630\mathrm{D}^2 + 0.831E^2 + 0.1710\mathrm{A} - 0.1921\mathrm{BD} \quad (4)$$

The capability of the developed predictive mathematical model was checked using a coefficient of determination R-Squares. The developed regression model for the specific heat capacity has a high coefficient of determination R-square, adjusted R-square, and

DOI 10.11113/jm.v48.509

predicted R-square values of 99.27%, 97.25%, and 88.12%, respectively. As per the studies conducted by Dan-Asabe *et al*. [49] and Sivaiah and Chakradh [50], an R-Square value greater than 75% is generally deemed acceptable, indicating a satisfactory fit between the process parameters and the responses. Figure 11 illustrates curves of the specific wear rate data generated using the model equation (Equation 4) and the experimental values for the 16 different runs.

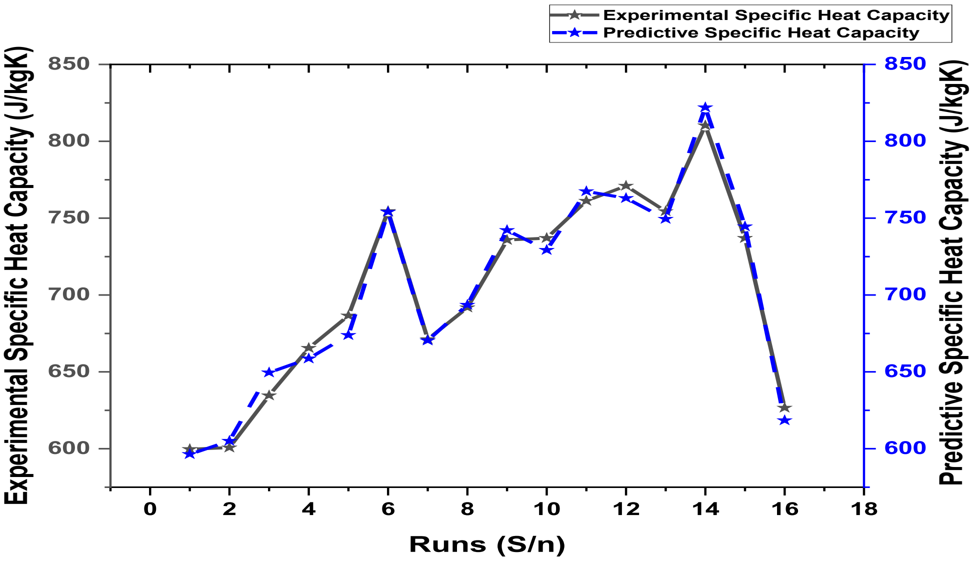

Figure 11: Experimental and predictive specific heat capacity

3.7 Confidence Interval (CI)

A confidence interval of ± 45.48 was evaluated using Equation 2. The experimental SHC (824.58 J/kgK) obtained from the confirmatory test falls within the confidence interval range of the specific wear rate, confirming the validity of the experimental result within the confidence interval of 95%, as illustrated below:

$$SHC_{predictive} - CI < SHC_{experimental} < SHC_{predictive} + CI$$
$$779.37 < SHC_{experimental} < 870.33$$

This result confirms the acceptability of the optimum specific heat capacity prediction within the confidence interval of 95%.

4.0 CONCLUSION

This study focuses on enhancement of the SHC of Al-BP-CA hybrid composites for brake disc applications through the modelling and optimization of double stir casting process parameters. The aluminum alloy, brown pumice, coal ash, and hybrid composites were successfully developed and characterized. This study led to the following conclusions:

i. The characterization results revealed that brown pumice and coal ash contained hard and stiff minerals such as SiO_2, Fe_2O_3, and Al_2O_3, making them suitable as reinforcements in metal matrixes such as aluminum, titanium, and magnesium.
ii. The thermogravimetric and differential thermal analyses demonstrated that the aluminum alloy, brown pumice, and coal can withstand high temperatures of up to 264.08, 724 °C, and 606.61°C, respectively, before any significant deterioration.
iii. The optimization process resulted in the achievement of optimal specific heat capacities of 824.85 J/kgK (experimental) and 820.48 J/kgK (predicted) by

utilizing 7.5 vol% of brown pumice, 5 vol% of coal ash, 400 rpm stirrer speed, 850 °C pouring temperature, and 20 minutes stirring duration.

iv. The developed mathematical model demonstrated an excellent level of prediction for the SHC of the composites based on the process parameters and ceramics reinforcement, with 99.27%, 97.25%, and 88.12%, as R-Square and adjusted R-Square, and predicted R-Square values, respectively.

ACKNOWLEDGEMENT

I owe a tremendous debt of gratitude to my dedicated and supportive thesis supervisors, Prof. D. S. Yawas, Prof. B. Danasabe, and Dr. A. A. Adebisi, whose unwavering guidance, expertise, and encouragement have been instrumental in shaping this research, your valuable insights and constructive feedback have enriched the quality of this work, and I am truly grateful for your mentorship.
.

CONFLICT OF INTEREST

The author declares that there is no conflict of interest regarding the publication of this paper.

REFERENCES

[1] Ibrahim, T. K., Yawas, D. S., Dan-asabe, B., & Adebisi, A. A. (2023). Manufacturing and optimization of the effect of casting process parameters on the compressive strength of aluminum/pumice/carbonated coal hybrid composites: Taguchi and regression analysis approach. *International Journal of Advance Manufacturing, 125*, 3401–3414. https://doi.org/10.1007/s00170-023-10923-2

[2] Nong, X., Jiang, Y., Fang, M., Yu, L., & Liu, C. (2017). Numerical analysis of novel SiC3D/Al alloy co-continuous composites ventilated brake disc. *International Journal of Heat and Mass Transfer, 108*, 1374–1382. https://doi.org/10.1016/j.ijheatmasstransfer.2016.11.108

[3] Adediran, A. A., Alaneme, K. K., Oladele, I. O., Akinlabi, E. T., & Sánchez, J. (2021). Microstructural characteristics and mechanical behavior of aluminum matrix composites reinforced with Si-based refractory compounds derived from rice husk. *Cogent Engineering, 8*(1). https://doi.org/10.1080/23311916.2021.1897928

[4] Ashok-Kumar, R., & Devaraju, A. (2021). Modeling of mechanical properties and high temperature wear behavior of Al7075/SiC/CRS composite using RSM. *Silicon, 13*, 3499–3519. https://doi.org/10.1007/s12633-020-00801-x

[5] Chandel, R., Sharma, N., & Bansal, S. A. (2021). A review on recent developments of aluminum-based hybrid composites for automotive applications. *Emergent Materials, 4*(5), 1243–1257.

[6] Adebisi, A. A., & Ndaliman, M. B. (2015). Mathematical modelling of stir casting process parameters for AlSicp composite using central composite design. *28th AGM and International Conference of the Nigerian Institution for Mechanical Engineers* (pp. 1–10). The Nigerian Institution for Mechanical Engineers.

[7] Arunkumar, T., Sreevatsa, K. A., Krishnan, D. R., & Subbiah, R. (2020). Corrosion behaviour of aluminium 6061/MWCNT composite prepared by double stir casting method. *International Conference on Advances in Materials Processing & Manufacturing Applications* (pp. 293–299). Springer.

[8] Vinod, B., Ramanathan, S., Ananthi, V., & Selvakumar, N. (2019). Fabrication and characterisation of organic and in-organic reinforced A356 aluminium matrix hybrid composite by improved double-stir casting. *Silicon, 11*(2), 817–829.

[9] Ochuokpa, E. O., Yawas, D. S., Okorie, P. U., & Sumaila, M. (2021). Evaluation of mechanical and metallurgical properties Al-Si-Mg/Mangiferaindica seed shell ash (MSSA) particulate composite for production of motorcycle hub. *Journal of Science Technology and Education, 9*(1), 221–238.

[10] Kumar, A., Rana, R. S., & Purohit, R. (2020). Effect of stirrer design on microstructure of MWCNT and Al alloy by stir casting process. *Advances in Materials and Processing Technologies, 6*(2), 320–327.

[11] Alabi, A. A., Samuel, B. O., Peter, M. E., & Tahir, S. M. (2022). Optimization and modelling of the fracture inhibition potential of heat treated doum palm nut fibres in phenolic resin matrix polymer composite: A Taguchi approach. *Functional Composites and Structures, 4*(1), 015004.

[12] Ibrahim, T. K., Yawas, D. S., Dan-asabe, B., & Adebisi, A. A. (2023). Optimization and statistical modeling of the thermal conductivity of a pumice powder and carbonated coal particle hybrid reinforced aluminum metal matrix composite for brake disc application: A Taguchi approach. *Functional Composite and Structure, 5*(1), 015008. https://doi.org/10.1088/2631-6331/acc0d1

[13] Ibrahim, T. K., Yawas, D. S., Dan-asabe, B., & Adebisi, A. A. (2023). Taguchi optimization and modelling of stir casting process parameters on the percentage elongation of aluminium, pumice and carbonated coal composite. *Scientific Reports, 13*, 2915. https://doi.org/10.1038/s41598-023-29839-8

[14] Zhou, H., Bhattarai, R., Li, Y., Si, B., Dong, X., Wang, T., & Yao, Z. (2022). Towards sustainable coal industry: Turning coal bottom ash into wealth. *Science of The Total Environment, 804*, 149985.

[15] Kumar, M. A., Seetharamu, S., Nayak, J., & Satapathy, L. (2014). A study on thermal behavior of aluminum cenosphere powder metallurgy composites sintered in microwave. *Procedia Materials Science, 5*, 1066–1074. https://doi.org/10.1016/j.mspro.2014.07.398

[16] Jayakrishnan, P., & Ramesan, M. T. (2016). Synthesis, characterisation and properties of poly (vinyl alcohol)/chemically modified and unmodified pumice composites. *Journal of Chemical and Pharmaceutical Sciences, 974*, 2115.

[17] Hassan, M., & Gomes, V. G. (2018). Coal derived carbon nanomaterials–Recent advances in synthesis and applications. *Applied Materials Today, 12*, 342–358.

[18] Sharma, A., Sakimoto, N., & Takanohashi, T. (2018). Effect of binder amount on the development of coal-binder interface and its relationship with the strength of the carbonised coal-binder composite. *Carbon Resources Conversion, 1*(2), 139–146.

[19] Kumar, R., & Kumar, V. (2017). Optimization of process parameter for Stir Casted AA6063 Metal Matrix Composite on Hardness, Tensile Strength and Impact Energy. *International Journal of Mechanical Engineering and Technology, 8*(12), 108–117.

[20] Patil, G., & Patil, M. H. (2020). Optimization of stir cast process parameters for better mechanical properties. *International Journal of Engineering Research & Technology, 9*(8), 482–486.

[21] Ikubanni, P. P., Oki, M., Adeleke, A. A., & Omoniyi, P. O. (2021). Synthesis, physico-mechanical and microstructural characterization of Al6063/sic/pksa hybrid reinforced composites. *Scientific Reports, 11*(1). https://doi.org/10.1038/s41598-021-94420-0

[22] Madhukar, P., Selvaraj, N., Gujjala, R., & Rao, C. S. P. (2019). Production of high performance AA7150-1% SiC nanocomposite by novel fabrication process of ultrasonication assisted stir casting. *Ultrasonics Sonochemistry, 58*, 104665.

[23] Advesh, B. (2011). *Development and property evaluation of aluminum alloy reinforced with nano-ZrO2 metal matrix composites (nmmcs) for automotive applications* [Doctoral dissertation, Dr. MGR Educational and Research Institute].

[24] Kok, M. (2005). Production and mechanical properties of Al2O3 particle-reinforced 2024 aluminium alloy composites. *Journal of Materials Processing Technology, 161*, 381–387.

[25] Ibrahim, T. K., Yawas, D. S., Thaddaeus, J., Danasabe, B., Iliyasu, I., Adebisi, A. A., & Ahmadu, T. O. (2024). Development, modelling and optimization of process parameters on the tensile strength of aluminum, reinforced with pumice and carbonated coal hybrid composites for brake disc application. *Scientific Reports, 14*(1), 16999. https://doi.org/10.1038/s41598-024-67476-x

[26] Ibrahim, T., Yawas, D. S., & Aku, S. Y. (2013). Effects of gas metal arc welding techniques on the mechanical properties of duplex stainless steel. *Journal of Minerals and Materials Characterization and Engineering, 1*, 222–230.

[27] Samuel, B. O., Alabi, A. A., Lawal, S. A., Peter, E., & Ibrahim, T. K. (2024). Optimizing the effect of heat treatment on the mechanical properties (tensile strength and hardness) of Hyphaene Thebaica nut; a machine learning and Taguchi approach. *Heliyon, 10*(19), e38899. https://doi.org/10.1016/j.heliyon.2024.e38899

[28] Verma, S., Kakkar, V., & Singh, H. (2022). Optimisation of cutting forces in dry turning process using Taguchi and grey relational analysis. *Recent Advances in Operations Management Applications* (pp. 317–334).

[29] Kareem, A., Qudeiri, J. A., Abdudeen, A., Ahammed, T., & Ziout, A. (2021). A review on AA 6061 metal matrix composites produced by stir casting. *Materials, 14*(1), 175. https://doi.org/10.3390/ma14010175

[30] Dagwa, I. M., & Adama, K. K. (2018). Property evaluation of pumice particulate-reinforcement in recycled beverage cans for Al-MMCs manufacture. *Journal of King Saud University-Engineering Sciences, 30*(1), 61–67.

[31] Ibrahim, T. K., Leva, I. U., Iliyasu, I., & Yawas, D. S. (2016). Comparative analysis of neem and lubricating (85W90) oils as quenchants on the mechanical properties of gas metal arc welded duplex stainless steel. *International Journal of Scientific and Engineering Research, 7*(4), 1825–1836.

[32] Gowda, B. M., Joshi, R., & Kuntanahal, R. (2020). Studies on bottom ash strengthened LM13 composite. *Materials Today: Proceedings, 20*, 217–221. https://doi.org/10.1016/j.matpr.2019.11.119

[33] Usman, Y., Dauda, E. T., Abdulwahab, M., & Dodo, R. M. (2020). Effect of mechanical properties and wear behaviour on locust bean waste ash (LBWA) particle reinforced aluminium alloy (A356 alloy) composites. *FUDMA Journal of Sciences (FJS), 4*(1), 416–421.

DOI 10.11113/jm.v48.509

[34] Ersoy, B., Sariisik, A., Dikmen, S., & Sariisik, G. (2010). Characterization of acidic pumice and determination of its electrokinetic properties in water. *Powder Technology, 197*, 129–135. https://doi.org/10.1016/j.powtec.2009.09.005

[35] Pınarcı, İ., & Kocak, Y. (2022). Hydration mechanisms and mechanical properties of pumice substituted cementitious binder. *Construction and Building Materials, 335*, 127528.

[36] Ibrahim, T. K., Iliyasu, I., & Abiodun, P. C. (2024). Application of Taguchi methods and regression analysis to optimize process parameters and reinforcements for maximizing composite's coefficient of friction for brake disc application: A statistical optimization approach. *Journal of Sustainable Materials Processing and Management, 4*(1), 89–105. https://publisher.uthm.edu.my/ojs/index.php/jsmpm/article/view/17768

[37] Gencel, O. (2015). Characteristics of fired clay bricks with pumice additive. *Energy and Buildings, 102*, 217–224. https://doi.org/10.1016/j.enbuild.2015.05.03

[38] Shetty, P., Vinay Atgur, V., Manavendra, G., & Naik, P. (2015). Experimental evaluation of specific heat carrying capacity of fly-ash. *International Research Journal of Engineering and Technology, 2*(9), 774–780.

[39] Hoff, B. W., Dynys, F. W., Hayden, S. C., Grudt, R. O., Hilario, M. S., Baros, A. E., & Ostraat, M. L. (2019). Characterization of AlN-based ceramic composites for use as millimeter wave susceptor materials at high temperature: High temperature thermal properties of AlN:Mo with 0.25% to 4.0% Mo by volume. *Materials Research Society, 1531–1542*. https://doi.org/10.1557/adv.2019.142

[40] Santhosh Kumar, B. M., Girish, D. P., Yogesha, K. B., & Jeevan, M. C. (2019). Influence of hybrid reinforcement on thermal conductivity of Al7075 based composites. *Materials Research Express, 6*(12). https://doi.org/10.1088/2053-1591/ab575a

[41] Hasan, B. M., Jalaluddin Tarakka, R., Syahid, M., Amijoyo, M. A., & Anis, I. R. (2024). Thermal properties characteristic of aluminium-alumina composite for solar water heating system application. *Journal of Physics: Conference Series, 2739*(1), 012018. https://doi.org/10.1088/1742-6596/2739/1/012018

[42] Cem Okumus, S., Aslan, S., Karslioglu, R., Gultekin, D., & Akbulut, H. (2012). Thermal expansion and thermal conductivity behaviors of Al-Si/SiC/graphite hybrid metal matrix composites (MMCs). *Materials Science, 18*(4), 341–346. https://doi.org/10.5755/j01.ms.18.4.3093

[43] Krishna, S. A. M., Shridhar, T. N., & Krishnamurthy, L. (2015). An experimental investigation on specific heat capacity and enthalpy of Al 6061-SiC-Gr hybrid metal matrix composites using differential scanning calorimetry. *Advanced Materials Research, 1105*, 208–214.

[44] Khosravi, H., Bakhshi, H., & Salahinejad, E. (2014). Effects of compocasting process parameters on microstructural. *Transactions of Nonferrous Metals Society of China, 24*(8), 2482–2488. https://doi.org/10.1016/S1003-6326(14)63374-4

[45] Malau, V., Wildan, M. W., Suyitno, & Sadi. (2014). Optimization of process parameters of stir casting to maximize the hardness of Al-SiC composites by Taguchi method. *International Journal of Applied Engineering Research, 9*(24), 30121–30134.

[46] Hashim, J., Looney, L., & Hashmi, M. S. J. (2001). The wettability of SiC particles by molten aluminium alloy. *Journal of Materials Processing Technology, 119*, 324–32.

[47] Ibrahim, T. K., Thaddaeus, J., Popoola, C. A., Iliyasu, I., & Alabi, A. A. (2024). Improvement of wear rate properties of a brown pumice and coal ash particulates reinforced aluminum composite for automobile brake manufacturing, through optimization and modelling. *Jordan Journal of Mechanical and Industrial Engineering, 81*(4). https://doi.org/10.59038/jjmie/180409

[48] Karthikeyan, B., Ramanathan, S., & Ramakrishnan, V. (2011). Specific heat capacity measurement of Al / SiCp composites by differential scanning calorimeter. *Advanced Materials Research, 264–265*, 669–674. https://doi.org/10.4028/www.scientific.net/AMR.264-265.669

[49] Dan-Asabe, B., Yaro, S. A., Yawas, D. S., & Aku, S. Y. (2019). Statistical modeling and optimization of the flexural strength, water absorption and density of a doum palm-Kankara clay filler hybrid composite. *Journal of King Saud University-Engineering Sciences, 31*(4), 385–394.

[50] Sivaiah, P., & Chakradhar, D. (2019). Modeling and optimization of sustainable manufacturing process in machining of 17-4 PH stainless steel. *Measurement, 134*, 142–152.

DOI 10.11113/jm.v48.509